RSC Advances

PAPER

View Article Online
View Journal | View Issue

Check for updates

Cite this: *RSC Adv.*, 2024, **14**, 39094

A low-toxicity uranyl-selective-binding linear pentapeptide sequence as a potential uranium decorporation agent†

Xiaohong Tan,[a] Libing Yu,[b] Xindan Liao,[b] Chun Chen,[b] Jian Chu,[b] Zhonghua Xiong,[b] Binyuan Xia,[b] Wei Tang, *[b] Xijian Li *[b] and Yanyan Liu *[a]

Received 26th August 2024
Accepted 4th December 2024

DOI: 10.1039/d4ra06173j

rsc.li/rsc-advances

Searching for highly selective, efficient, and low-toxicity chelating agents is central to resolving uranium contamination *in vivo*. Peptides composed of amino acids exhibit very low toxicity for accumulation in the human body and have been proven effective in chelating actinides within the human body. Herein, we report a rationally designed short phosphorylated peptide sequence **PP-B**, which exhibits high affinity and selectivity for uranyl compared to other trace elements present in the body (such as Na^+, K^+, Ca^{2+}, Co^{2+}, Fe^{2+}, Fe^{3+}, Mg^{2+}, Mn^{2+}, Zn^{2+}). The association constant for the peptide–uranyl complex is calculated to be 7.3 $\times 10^5$ M^{-1}. The result of DFT calculation shows that the phosphate group binds strongly to the UO_2^{2+} center, potentially accounting for the peptide's strong affinity towards UO_2^{2+}. The results of *in vivo* uranyl decorporation assays reveal that **PP-B** has a much lower toxicity and a much higher decorporation efficiency than that of the clinically approved DTPA. These findings render **PP-B** a promising candidate for utilization as a novel decorporation agent.

1 Introduction

Uranium is the key element for nuclear-energy production, and its utilization in many other applications has been increasing.[1] Nevertheless, uranium's radioactivity and chemical toxicity pose significant risks.[2–4] Uranium primarily induces health problems *via* poisoning kidneys (36.22%), bone (19.48%), liver (17.58%), the reproductive system (13.90%), lungs (7.24%), and the nervous system (5.58%). As an important nephrotoxicant, the site-specific accumulation of uranium in the proximal tubules may cause proximal tubular damage and renal failure. The mechanisms underlying the toxicological effects caused by uranium have been extensively studied. Recent advances have focused on oxidative stress, genetic damage, protein injury, cell apoptosis, inflammation, and metabolic disorders.[5,6] The recommended clinical treatment for internal uranium contamination involves the infusion of 250 mL of sodium bicarbonate solution (1.4%). However, the intravenous injection of large quantities of sodium bicarbonate can upset the body's acid–base balance, potentially leading to hypokalemia, alkalosis, or other health issues.[7–13] Diethylenetriamine pentaacetate (DTPA) is a clinically approved actinide chelator, yet its efficacy in uranium excretion is limited due to its low affinity for uranyl, poor membrane permeability, and mismatched ligand environment.[14,15] Chelators containing hydroxypyridone (HOPO), terephthalamide (TAM), and catechol (CAM) functional groups have shown promise in actinide decomposition, but most CAM- and TAM-based ligands have been found to be toxic and may damage the kidney, liver and/or spleen.[16–19] Based on the characteristics of porous organic, which offer tunable functional groups, high surface area, and large porosity, they are extensively applied for the extraction and purification of uranium solutions. Dr Juan Diwu's team successively synthesized carboxyl-functionalized nanoscale metal organic frameworks (nMOFs) (UiO-66-$(COOH)_4$),[20] HOPO-functionalized nMOFs (MIL-101-HOPO)[21] and carboxyl-functionalized nMOFs (ZIF-71-COOH),[22] as well as CON-AO obtained by attaching amidoxime (AO) groups to the channels of covalent organic sheets (CON),[23] which greatly improves the selectivity and affinity for uranium. However, toxicity studies on nanomaterials are scarce, and deeper investigations into their degradation mechanisms and associated side effects on normal organs are necessary.[24] Despite substantial research progress in the field of uranium prokinetics, the development of effective chelators with high selectivity and low toxicity towards uranium, possessing both high oral bioavailability and low cost for clinical use, remains a pending challenge.

Uranium predominantly exists under its main oxidation state +VI with two axial oxo ligands which form the linear triatomic uranyl ion with an overall charge of +II. The ability to afford four to six equatorial ligands in octahedral, pentagonal or

[a]School of Safety Science and Emergency Management, Wuhan University of Technology, Wuhan, 430070, China

[b]Institute of Materials, China Academy of Engineering Physics, Jiangyou, Mianyang, Sichuan 621907, China

† Electronic supplementary information (ESI) available. See DOI: https://doi.org/10.1039/d4ra06173j

Open Access Article. Published on 10 December 2024. Downloaded on 2/10/2026 4:59:52 AM. This article is licensed under a Creative Commons Attribution-NonCommercial 3.0 Unported Licence.

© 2024 The Author(s). Published by the Royal Society of Chemistry

Open Access Article. Published on 10 December 2024. Downloaded on 2/10/2026 4:59:52 AM. This article is licensed under a Creative Commons Attribution-NonCommercial 3.0 Unported Licence.

hexagonal bipyramidal geometries separates uranyl from most of the alkali, alkaline and transition metals.[25,26] Proteins act as the primary transporters of uranyl ion in the body. Several studies have identified proteins, including transferrin, osteopontin, albumin, globulin, and fetuin, that display a strong affinity for uranyl ions.[27,28] In 2014, He *et al.* reported that carboxylic acid side-chain ligands on proteins can form fivefold or sixfold planar coordination around the central uranyl, showing high selectivity and affinity for uranium.[29] Mimicking these proteins to design small peptide ligands may be an effective strategy for rationalize uranium–protein interactions.[29,30] Delangle *et al.* reported an engineered cyclodecapeptide with four glutamate residues to coordinate uranyl at the dioxo cation's equatorial plane, resulting in high affinity for uranyl. However, the high affinity of carboxyl groups with a variety of metal ions complicates the specific recognition of uranyl cation from numerous competing ions.[31] In 2015, Wang *et al.* discovered that phosphorylated cyclodipeptide exhibited high selectivity and sensitivity toward uranyl ions, which was successfully employed as a fluorescent sensor for the detection of uranyl ions in river water.[32] Recently, Delangle *et al.* employed similar strategy by using phosphate group in the cyclic peptide skeleton to achieve high affinity towards uranyl ion.[33–35] Mechanism studies have showed that phosphorylated functional groups and a pre-organized structure are critical structural parameters.[36,37]

Cyclic peptides are structurally constrained and could result in higher thermodynamic stability in cyclic peptide–uranyl complex. Consequently, cyclic peptides generally exhibit greater affinity and selectivity for uranyl than do linear peptides.[32] In contrast, linear peptides may be simpler and less expensive to utilize in practical applications. But the structure flexibility makes it a great challenge to obtain high affinity and selectivity towards uranyl. Le Clainche *et al.*[35] synthesized a 33-amino acid peptide corresponding to the helix-loop-helix motif of the calcium binding site I of the protein calmodulin from *Paramecium tetraurelia* and demonstrated that mutation of two aspartic acid residues in the peptide sequence gave access to a new peptide, which was selective for the uranyl ion.

In this study, we designed the short straight-chain pentapeptide **PP-B** as a model peptide (Fig. 1), which is more stable compared to long linear polypeptide chains (the synthesis steps are described in ESI†). To our knowledge, the designed pentapeptide **PP-B** is the shortest linear peptide sequence capable of uranium decorporation. The symmetrical design of the peptide structure enhances its stability in chelation with uranyl. Tyrosine produces natural fluorescence when excited by 280 nm excitation light and can be used as a fluorescent probe. In order to improve the high selectivity and sensitivity of the peptide to uranyl ions, we phosphorylated one of the threonine and tyrosine. UO_2^{2+} tends to coordinate with 4–6 binding sites on its equatorial plane, and based on this, we plan that **PP-B** can provide 3–4 coordination sites (which can be provided by the phosphate, phenolic hydroxyl, and carboxyl groups on the side chain), and the other 1–2 sites can be provided by water molecules in the system. The results indicate that **PP-B** shows a significant improvement in affinity compared to the non-phosphorylated peptide **PP-A**. These findings might illuminate the importance of phosphoamino acids in uranyl binding in proteins and the relevance of considering phosphoproteins as potential uranyl targets *in vivo*.

2 Experimental materials and methods

2.1 Experimental materials

Uranyl nitrate was purchased from Hubei Chushengwei Chemical Ltd (Hubei, China). Diethylenetriaminepentaacetic acid (DTPA) was purchased from Macklin Biochemical Co., Ltd (Shanghai, China). 4-(2-Hydroxyethyl)1-piperazineethanesulfonic acid (HEPES, ≥99.0%) was purchased from Sangon Biotech Co., Ltd (Shanghai, China). Sodium bicarbonate and other salts solution was purchased from TCI Development Co., Ltd (Shanghai, China). HK-2 cells, fetal bovine serum (FBS) and DMEM/F-12 medium were purchased from Wuhan Procell Life Science & Technology Co., Ltd (Wuhan, China). Cell Counting Kit-8 (CCK-8) assay kit were purchased from Beyotime Biotech Inc (Shanghai, China). All reagents were analytically pure. Ultrapure water obtained using the Direct-Q5 purification system (Bausasi Technology, 18.2 MΩ cm^{-1} resistivity) was used in all experiments.

Shimadzu LC-20AP preparative liquid chromatography (Shimadzu, Japan) was utilized in conjunction with Thermo Fisher Orbitrap Astral mass spectrometer detector (Thermo Fisher, USA) for peptide purification and structural characterization. Fluorescence spectral data for the peptides were recorded using a HORIBA Fluoromax-4 molecular fluorescence spectrometer (Horiba, France). Cell viability was measured using a luminescence detection at 450 nm on a SpectraMax i3x multifunctional enzyme marker instrument (Molecular, USA).

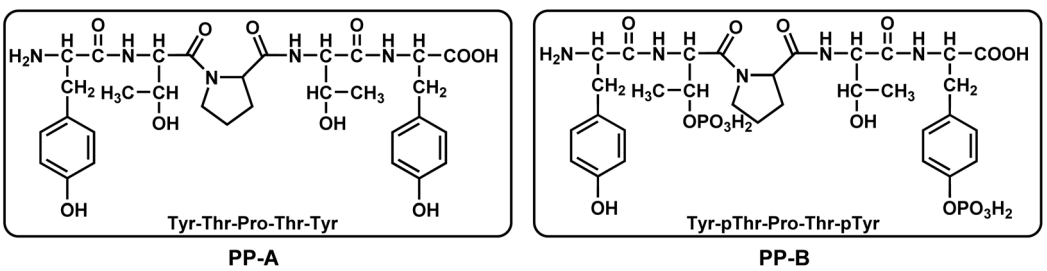

Fig. 1 Structure of linear pentapeptide PP-A and PP-B.

Open Access Article. Published on 10 December 2024. Downloaded on 2/10/2026 4:59:52 AM. This article is licensed under a Creative Commons Attribution-NonCommercial 3.0 Unported Licence.

2.2 Characterization

The phosphorylated peptide was purified and characterized by high performance liquid chromatography (HPLC) and mass spectrometry (ESI-MS). High-resolution mass spectra were collected under the specific conditions (ESI+ spray voltage, 4.5 kV; nebulizer gas, 1.5 L min^{-1}; heat block temperature, 200 °C; CDL temperature, 200 °C; detector voltage, 1.5 kV. The source settings were the same for both samples to get comparable data).

2.3 Fluorescence titration experiment

In order to verify that the introduction of the phosphate group plays an important role in enhancing the chelating ability of uranium ions, the non-phosphorylated polypeptide (**PP-A**) was set up as a comparison with the phosphorylated polypeptide (**PP-B**). The fluorescence spectra of the two polypeptides were measured in a four-side translucent quartz cuvette. A stock uranyl solution (2 mM) was prepared from uranyl nitrate in nitric acid (0.01 M). HEPES buffer (0.01 M) was prepared by dissolving solid 4-(2-hydroxyethyl)-1-piperazineethanesulfonic acid in ultrapure water. Peptide solution (20 μM) was freshly prepared by dissolving peptide solid in 0.01 M HEPES buffer, followed by pH adjustment to 7.0 with KOH. Tyrosine fluorescence quenching was followed by titration of the peptide buffered solution with a certain equivalent of uranyl. The pH was measured at the beginning and at the end of the experiment to guarantee pH stability during titration. The measurements were performed at 25 °C. Tyrosine fluorescence was excited at 275 nm (with an excitation slit of 5.0 nm) and the emission slit was adjusted (5 nm) to avoid signal saturation. The binding constants for peptide–UO_2^{2+} chelates were calculated using the BindFit v0.5 algorithm.

2.3.1 Metal ion selectivity experiment. The selective chelating ability of metal ions by phosphorylated peptides was also determined by fluorescence titration experiments. Fluorescence spectral data were obtained by HORIBA Fluoromax-4. 10 μL of 2 mM solutions of various metal ions (Na^+, K^+, Ca^{2+}, Co^{2+}, Fe^{2+}, Fe^{3+}, Mg^{2+}, Mn^{2+}, Zn^{2+}, UO_2^{2+}, Ag^+, Al^{3+}, Pb^{2+}) were added to a 2 mL solution of 20 μM phosphorylated peptide sample, and the remaining conditions were consistent with those described above. The ability of the phosphorylated peptide to selectively chelate UO_2^{2+} was determined by comparing the fluorescence intensities.

2.3.2 Job's plot experiment. Job's plot working curve can be used to explore the complexation ratio of phosphorylated peptide with uranyl ions. The total concentration and volume of peptide and uranium were kept constant at 20 μM and 2 mL, respectively. The ratio of peptide and uranium in the solution was changed to obtain the measured solution, fluorescence values I were measured at 302 nm, and the pre-reaction fluorescence values I_0 of the same ratio of peptide-only solutions were also determined. The Mole ratio plot was plotted using Origin software to determine the chelation ratio of peptide–UO_2^{2+} complex.

2.4 Density functional theory (DFT) calculation

The structure was optimized by using the DFT approach as implemented in the Gaussian 16 software. The B3LYP functional[38] and mixed basis set (SDD ECP basis set for U atom and the 6-31G (d, p) basis set for other atoms) were adopted for geometry optimization and frequency calculations, and the optimal geometry for each compound was determined. The DFT-D3 dispersion correction[39] was applied to correct the weak interaction to improve the calculation accuracy. The SMD implicit solvation model[40] was used to account for the solvation effect.

2.5 *In vitro* cells assay

The HK-2 cell line was cultured in a medium containing a mixture of F-12 nutrient mixture (DMEM/F-12), 10% (v/v) fetal bovine serum (FBS), and 1% penicillin–streptomycin in a humidified atmosphere of 5% CO_2 at 37 °C. The cells were propagated every two days. The medium used for poisoning had the proportion of FBS adjusted from 10% to 3%. Cells for measurement were cultured in clear 96-well plates at a density of 8×10^3 HK-2 cells and incubated with 100 μL of medium per well.

2.5.1 Solution preparation. PP-B (10 mM), DTPA (10 mM), uranyl nitrate solution (100 mM), sodium bicarbonate (1 M) was prepared from solid in ultrapure water. Uranyl nitrate (100 mM), sodium bicarbonate (1 M) and ultrapure water were ultrasonically mixed in the ratio of 1 : 1 : 8 to obtain 10 mM uranyl carbonate solution. All solutions were sterilized by 0.22 μm sterilization filter. The work solutions containing chelating agent and U(VI) were prepared by diluting with culture medium to the expected concentrations for cell treatment.

2.5.2 Cell toxicity and detoxification assays. To investigate the cytotoxicity of phosphorylated peptides on human cells and the decorporation effect on uranium-contaminated toxic cells, the clinically approved chelating agent DTPA was used as a control.[41] Cell viability was assessed by the CCK-8 assay, with 6 parallel samples per group. For cytotoxicity evaluation, exponentially growing HK-2 cells were cultured for 24 h and then exposed to poisoning medium with varying concentrations of chelating agents (0 μM, 100 μM, 200 μM, 400 μM, 600 μM, 800 μM) in the experimental groups. For uranium decorporation assays, the early administration group (**PP-B** + U), the timely administration group (**PP-B** − U) and the delayed administration group (U + **PP-B**) were set up. For each group, 800 μM U(VI) and different concentrations of chelating agents (50 μM, 100 μM, 200 μM, 400 μM, 600 μM, 800 μM) were added to the experimental group, only 800 μM U(VI) was added to the control group. An increased relative level of viability correlates positively with the enhancement of detoxification effects. Before testing, the 96-well plate was incubated in the dark at 37 °C for 2 h after adding 10 μL of CCK-8 solution to each well. The absorbance at 450 nm was determined on a microplate reader. Relative level of viability = OD of experimental group/OD of control group.

3 Results and discussion

3.1 Characterization of peptides

The HPLC chromatogram of **PP-A** showed the peak at 9.640 minutes, with a purity of 99.64%. ESI-MS indicated that the relative molecular mass (RMM) of **PP-A** was 643.68. The HPLC

 © 2024 The Author(s). Published by the Royal Society of Chemistry

Open Access Article. Published on 10 December 2024. Downloaded on 2/10/2026 4:59:52 AM.
This article is licensed under a Creative Commons Attribution-NonCommercial 3.0 Unported Licence.

chromatogram of **PP-B** showed the peak at 11.563 minutes, with a purity of 98.84%. The RMM of **PP-B** is 803.64. Relatively images were shown in ESI.†

3.2 Mechanisms of uranyl-selective-binding linear pentapeptide

3.2.1 Binding constants of peptides to uranium. The fluorescence of tyrosine was previously demonstrated to serve as an effective probe to demonstrate uranyl complexes formation and to measure their conditional stability constants.[42,43] The fluorescence emission spectra were recorded at the excitation wavelength of 275 nm and the scatter plots are obtained in Fig. 2. Fluorescence titration experiments revealed that the fluorescence of **PP-B** was progressively quenched with the continuous addition of UO_2^{2+}, reaching almost complete quenching upon the addition of 3 equivalents. This result indicates that **PP-B** forms a stable chelation with UO_2^{2+}. Whereas **PP-A** exhibited only weak fluorescence quenching when 20 equivalents of uranium were added. The binding constant of **PP-B**–UO_2^{2+} complex was 7.3 $\times 10^5$ M^{-1} calculated by Bindfit v5.0, which was two orders of magnitude larger than that of **PP-A**–UO_2^{2+} complex (2.7 $\times 10^3$ M^{-1}). These findings suggest that phosphate groups play a crucial role in promoting the chelating ability of peptide sequences with UO_2^{2+}.

3.2.2 Metal-ion selectivity of peptide. Fig. 3 presents the results of fluorescence titration experiments involving **PP-B** and common metal ions (Na^+, K^+, Ca^{2+}, Zn^{2+}, Fe^{2+}, Fe^{3+}, Mg^{2+}, Cu^{2+}, Co^{2+}, *etc.*). The **PP-B** alone showed strong fluorescence intensity. Interestingly, when one equivalent of other metal ions (Na^+, K^+, Ca^{2+}, Zn^{2+}, Fe^{2+}, Fe^{3+}, Mg^{2+}, Cu^{2+}, Co^{2+}, *etc.*) were added to the **PP-B** solution, the fluorescence emission at 302 nm was not significantly affected. In contrast, the introduction of one equivalent of uranyl ions induced a significant fluorescence

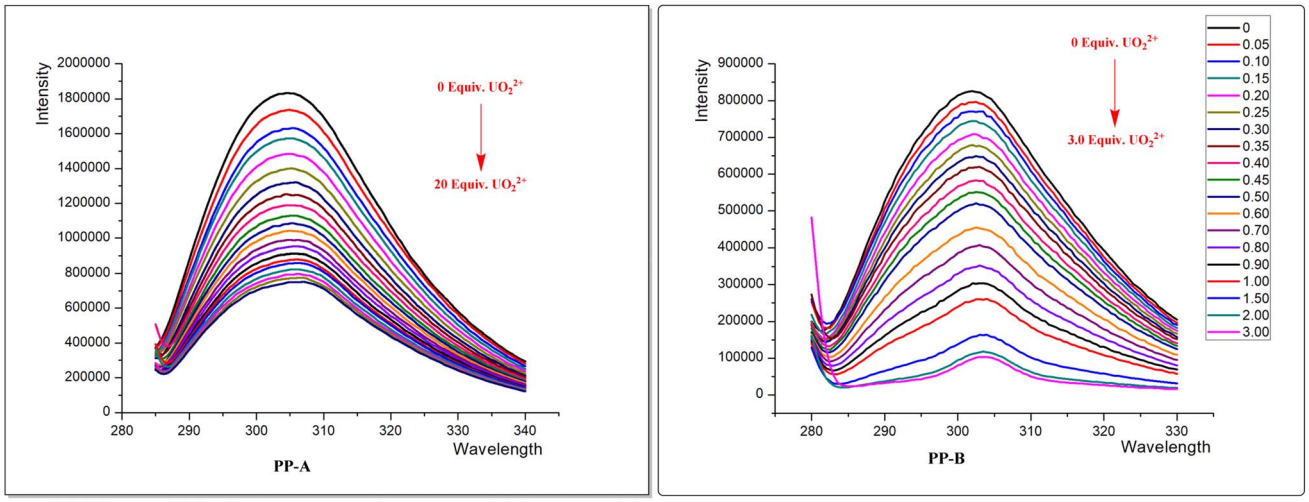

Fig. 2 Fluorescence titration of PP-A and PP-B.

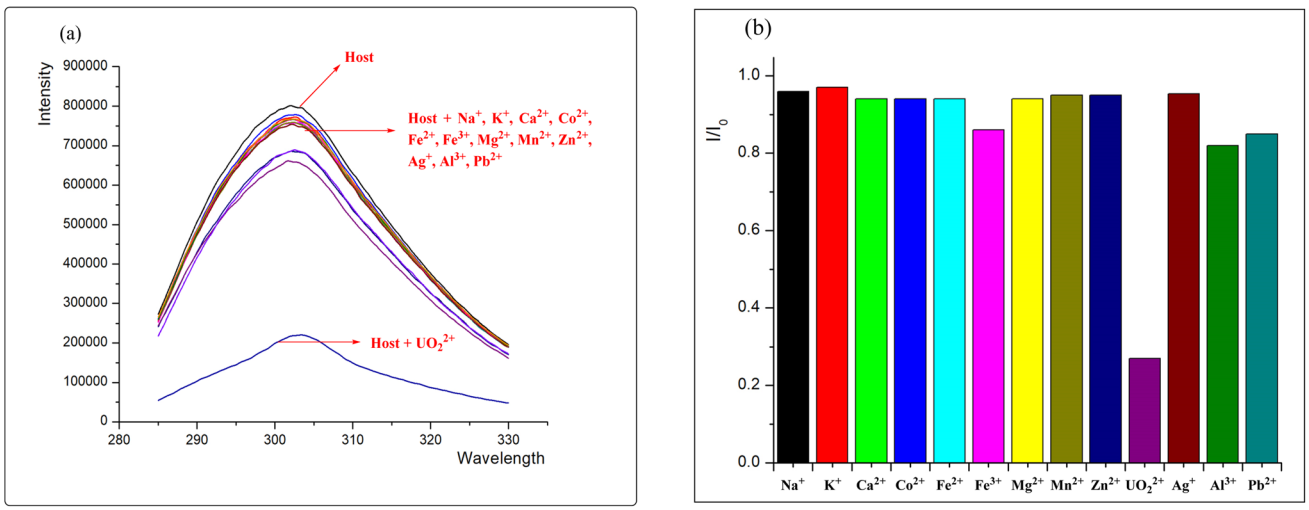

Fig. 3 (a) Fluorescent responses of PP-B (20 μM) to metal ions (1.0 equiv.) at pH 7.0, HEPES buffer (1 mM), with excitation at 275 nm. (b) The bar graphs of the fluorescence intensity at $\gamma = 302$ nm.

Open Access Article. Published on 10 December 2024. Downloaded on 2/10/2026 4:59:52 AM. This article is licensed under a Creative Commons Attribution-NonCommercial 3.0 Unported Licence.

quenching, with a quenching rate exceeding 70%, whereas the quenching rates for other metal ions were all below 15% shown in Fig. 3b. These results suggest that the straight-chain phosphorylated peptide possesses the ability to selectively chelate UO_2^{2+}. Consequently, **PP-B** emerges as a bio-friendly decorporation agent for uranium, without causing deficiencies of common metallic elements in the body.

3.2.3 Ratio of peptide binding to uranium. Under constant conditions of 20 μM total molar mass for the peptide–uranium mixture and a 2 mL total volume, the solutions were prepared with various binding ratios, and the Job's working curve was plotted according to the measured fluorescence values (Fig. 4). In the curve, the plot revealed that the fluorescence intensity was maximized when the molar fraction of phosphorylated peptide was 0.5, indicating that the phosphorylated peptide was 1 : 1 complexed with uranyl ion.

3.2.4 DFT structure optimization. Based on the results of Job's experiments which concluded that **PP-B** forms a 1 : 1 complex with uranyl, we have performed DFT optimizations on the proposed UO_2^{2+}–phosphate peptide complex. As is shown in Fig. 5, the U center adopts an octahedral geometry, with two oxygen atoms (UO_2^{2+}) on the apical position and four oxygen atoms (two from phosphate, one from Tyr and one from water molecule) on the equatorial plane. The bond distances for the four equatorial U–O single bond range from 2.354 Å to 2.607 Å, which is in good consistency with previously reported U(VI) complexes.[44] DFT calculations imply that the phosphate group binds strongly to the UO_2^{2+} center ($U\text{–}O^1 = 2.354$ Å and $U\text{–}O^3 = 2.349$ Å) and might explain why the phosphate peptide has strong affinity to UO_2^{2+}. Relatively unstable conformation is shown in ESI.†

3.3 *In vivo* uranyl decorporation

In the cytotoxicity assay, the cytotoxicity of **PP-A**, **PP-B** and DTPA exhibited a concentration-dependent increase (Fig. 6a). The survival rates of the cells remained above 80% even when the concentrations of **PP-A** and **PP-B** were increased to 1000 μM, which were significantly higher than that of DTPA, indicating that the cytotoxicity of **PP-A** and **PP-B** was significantly less than that of the clinically approved DTPA. This indicated that peptide chelators, with less toxic side effects resulting from accumulation in the human body, are bio-friendly drugs compared to DTPA.

In the decorporation assay, the timely/delayed treatment group exhibited the most significant overall enhancement in cell viability (Fig. 6c and d), with a cell viability value that was 2.5 times higher when 400/800 μM **PP-B** solution was added compared to the control group. The addition of **PP-A** has little effect. However, the addition of DTPA solution not only failed to increase the cell viability of uranium, but also had a toxic effect on the cells, decreasing the cell viability, and the toxicity increased with the increase of the concentration of DTPA. Additionally, the early administration group also exhibited an enhancement in cell viability (Fig. 6b), with a cell viability value that was 1.9 times higher when 800 μM **PP-B** solution was added compared to the control group. The addition of **PP-A** and DTPA had no beneficial effect. Thus, the timely and delayed treatment with **PP-B** provided the optimal removal effect for uranium contamination, and early pre-treatment potentially reduced uranium burden. The use of **PP-B** as a promotional excretion agent significantly increased cell viability compared to **PP-A** and DTPA, suggesting that the phosphorylation greatly enhances the ability of **PP-B** to bind to uranium, whereas DTPA exhibits

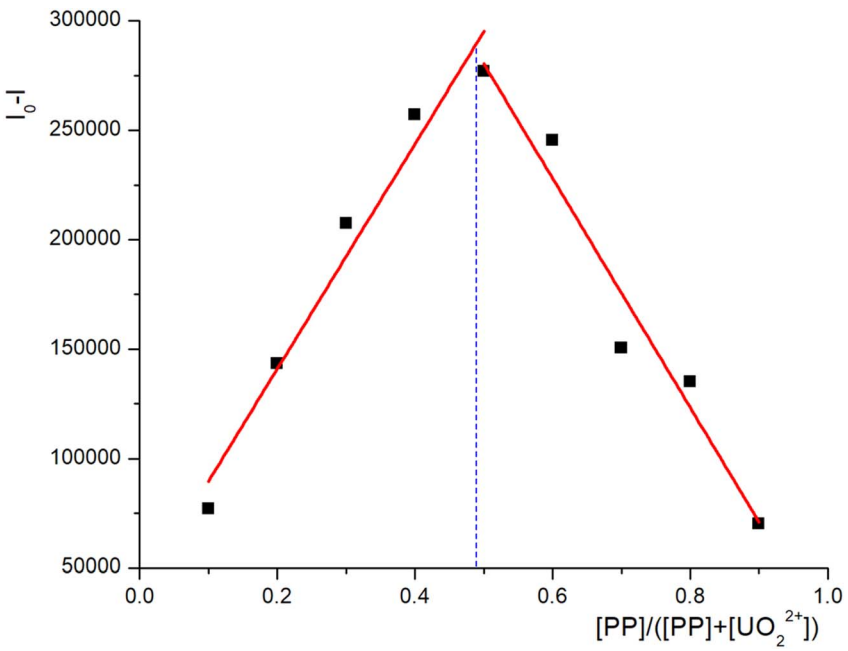

Fig. 4 Job's plot of **PP-B** with UO_2^{2+} representing stoichiometry 1 : 1.

© 2024 The Author(s). Published by the Royal Society of Chemistry

Open Access Article. Published on 10 December 2024. Downloaded on 2/10/2026 4:59:52 AM.
This article is licensed under a Creative Commons Attribution-NonCommercial 3.0 Unported Licence.

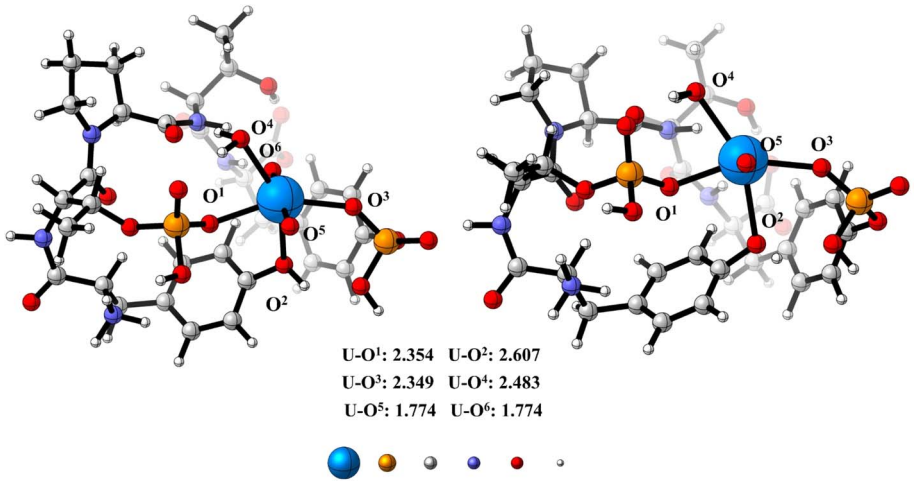

Fig. 5 Optimized structure of the UO_2^{2+}–**PP-B** complex from DFT calculations.

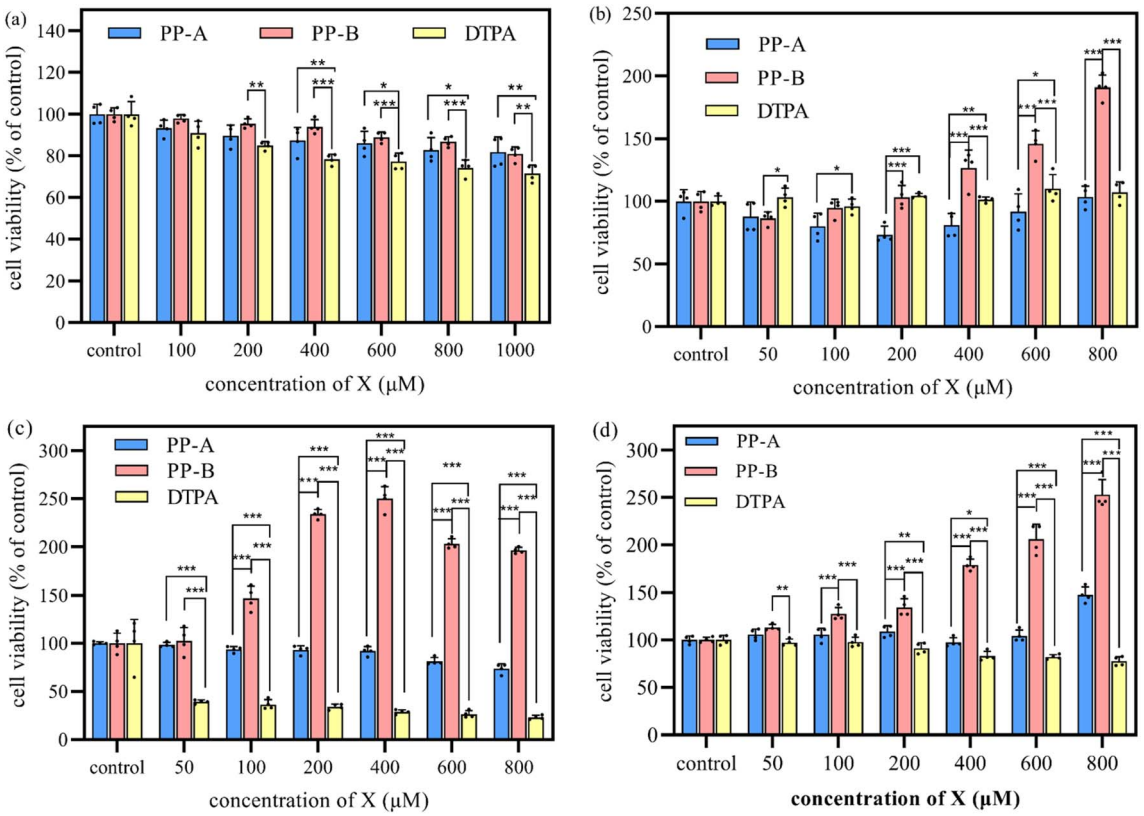

Fig. 6 (a) Effect of **PP-B** and DTPA on cell viability. Effect of **PP-B** and DTPA on the viability of uranium-stained HK-2 cells, (b) the early administration group (c) the timely administration group (d) the delayed administration group. *p < 0.05, **p < 0.01, ***p < 0.001.

minimal pro-excretion activity and slightly reduced cell viability.

4 Conclusion

In conclusion, the phosphorylated peptide **PP-B**, bearing the well preorganized donor structure matching the uranyl coordination environment, shows a higher binding constant for UO_2^{2+} compared to the unphosphorylated peptide. This study, along with prior investigations, verifies that the incorporation of a phosphate group serves as a viable strategy to enhance the chelating ability of UO_2^{2+}. *In vitro* cellular experiments have shown that **PP-B** exhibits significantly lower cytotoxicity than clinically used DTPA, with the cell survival rates consistently above 80%. **PP-B** demonstrated a higher uranyl-removing efficiency than **PP-A** and DTPA. The phosphorylated peptide is

Open Access Article. Published on 10 December 2024. Downloaded on 2/10/2026 4:59:52 AM. This article is licensed under a Creative Commons Attribution-NonCommercial 3.0 Unported Licence.

a short, straight-chain one and is facile to synthesize. Coupled with its selective binding ability, high efficiency and low cytotoxicity, the structure of this uranyl-selective-binding linear pentapeptide sequence is one of the most promising U(VI) decorporation agents and its practical application is expected to be realized in the future.

Data availability

The data presented in this study are available on ESI.†

Author contributions

Xiaohong Tan: methodology, experiment, software, formal analysis, investigation, writing – original draft, writing – review & editing; Libing Yu: experiment, project administration, writing – review & editing; Xindan Liao: conceptualization, methodology; Chun Chen: investigation, methodology; Jian Chu: methodology, experiment; Zhonghua Xiong: supervision, writing – review & editing; Binyuan Xia: supervision, writing – review & editing; Wei Tang: resources, writing – review & editing; Xijian Li: conceptualization, methodology, experiment, formal analysis, investigation, writing – original draft, writing – review & editing, funding acquisition, supervision, project administration.; Yanyan Liu: writing – review & editing.

Conflicts of interest

The authors declare that they have no known competing financial interests or personal relationships that could have appeared to influence the work reported in this paper.

Acknowledgements

We would like to acknowledge National Natural Science Foundation of China (22106149) for funding this work.

References

1 N. Hu, D. Ding, S. Li, X. Tan, G. Li, Y. Wang and F. Xu, *J. Environ. Radioact.*, 2016, **154**, 60–67.
2 É. Ansoborlo, B. Amekraz, C. Moulin, V. Moulin, F. Taran, T. Bailly, R. Burgada, M.-H. Hengé-Napoli, A. Jeanson, C. Den Auwer, L. Bonin and P. Moisy, *C. R. Chim.*, 2008, **10**, 1010–1019.
3 É. Ansoborlo, O. Prat, P. Moisy, C. Den Auwer, P. Guilbaud, M. Carriere, B. Gouget, J. Duffield, D. Doizi, T. Vercouter, C. Moulin and V. Moulin, *Biochimie*, 2006, **88**, 1605–1618.
4 O. Carugo, *J. Inorg. Biochem.*, 2018, **189**, 1–6.
5 M. Ma, R. Wang, L. Xu, M. Xu and S. Liu, *Environ. Int.*, 2020, **145**, 106107.
6 J. C. Liandong Zhang, B. Xia, Z. Xiong, S. Zhang and W. Tang, *Toxics*, 2022, **10**, 575.
7 J. W. Howland, *At. Energy Biophys. Biol. Med.*, 1948, **1**, 174.
8 Y. Ohmachi, T. Imamura, M. Ikeda, E. Shishikura, E. Kim, O. Kurihara and K. Sakai, *J. Toxicol. Pathol.*, 2015, **28**, 65–71.
9 M. H. Bhattacharyya, B. D. Breitenstein, H. Metivier, B. A. Muggenburg, G. N. Stradling and V. Volf, *Radiat. Prot. Dosim.*, 1992, **41**, 1–42.
10 T. Fujii, A. Udy, E. Licari, L. Romero and R. Bellomo, *J. Crit. Care*, 2019, **51**, 184–191.
11 T. Y. Yang, H. M. Lin, H. Y. Wang, M. H. Chuang, C. C. Hsieh, K. T. Tsai and J. Y. Chen, *Clin. J. Am. Soc. Nephrol.*, 2024, **19**, 959–969.
12 D. P. Hickman, *Radiat. Prot. Dosim.*, 2010, **141**, 215–216.
13 National Health Commission of the People's Republic of China, *Medical Management Standard for Internal Contamination of Radionuclides*, WS/T 583—2017, Standards Press of China, Beijing, 2017.
14 E. Fattal, N. Tsapis and G. Phan, *Adv. Drug Delivery Rev.*, 2015, **90**, 40–54.
15 A. E. V. Gorden, J. Xu, K. N. Raymond and P. Durbin, *Chem. Rev.*, 2003, **103**, 4207–4282.
16 Y. Bao, D. Wang, Z. Li, Y. Hu, A. Xu, Q. Wang, C. Shao and H. Chen, *Toxicol. Appl. Pharmacol.*, 2013, **269**, 17–24.
17 P. Durbin, B. Kullgren, J. Xu and K. Raymond, *Health Phys.*, 1997, **72**, 865–879.
18 Q. Zhang, B. Jin, T. Zheng, X. Tang, Z. Guo and R. Peng, *Inorg. Chem.*, 2019, **58**, 14626–14634.
19 B. Chen, S. Hong, X. Dai, X. Li, Q. Huang, T. Sun, D. Cao, H. Zhang, Z. Chai, J. Diwu and S. Wang, *J. Am. Chem. Soc.*, 2022, **144**, 11054–11058.
20 D. X. Wang, L. Chen, Z. Bai, D. D. Zhang, J. Guan, Y. Zhang, C. Shi and P. D. J. Diwu, *Angew. Chem.*, 2021, **133**, 1670–1674.
21 M. Chen, L. Lang, L. Chen, X. Wang, C. Shi, Q. Sun, Y. Xu, J. Diwu and S. Wang, *Chin. J. Chem.*, 2022, **40**, 2054–2060.
22 L. Chen, X. Wang, M. Chen, Q. Sun, Y. Chen, X. Zhang, R. Hong, Y. Xu, J. Guan, S. Hong, D. Cao, T. Sun, X. Li, L. Chen and J. Diwu, *Adv. Healthcare Mater.*, 2023, **12**, 2300510.
23 L. Chen, R. Bai, X. Wang, Y. Zhang, L. He, M. Zhang, Y. Chong, Z. Chai, X.-F. Wang and J. Diwu, *ACS Appl. Bio Mater.*, 2020, **3**, 8731–8738.
24 Y. Sun, L. Zheng, Y. Yang, X. Qian, T. Fu, X. Li, Z. Yang, H. Yan, C. Cui and W. Tan, *Nano-Micro Lett.*, 2020, **12**, 103.
25 J. Vanhorn and H. Huang, *Coord. Chem. Rev.*, 2006, **250**, 765–775.
26 A. Garai and P. Delangle, *J. Inorg. Biochem.*, 2020, **203**, 110936.
27 S. Safi, G. Creff, A. Jeanson, L. Qi, C. Basset, J. Roques, P. L. Solari, E. Simoni, C. Vidaud and C. Den Auwer, *Chemistry*, 2013, **19**, 11261–11269.
28 M. Starck, N. Sisommay, F. A. Laporte, S. Oros, C. Lebrun and P. Delangle, *Inorg. Chem.*, 2015, **54**, 11557–11562.
29 L. Zhou, M. Bosscher, C. Zhang, S. Özçubukçu, L. Zhang, W. Zhang, C. J. Li, J. Liu, M. P. Jensen, L. Lai and C. He, *Nat. Chem.*, 2014, **6**, 236–241.
30 M. R. Beccia, S. Sauge-Merle, N. Brémond, D. Lemaire, P. Henri, C. Battesti, P. Guilbaud, S. Crouzy and C. Berthomieu, *Biomolecules*, 2022, **12**, 1703.
31 C. Lebrun, M. Starck, V. Gathu, Y. Chenavier and P. Delangle, *Chem.–Eur. J.*, 2014, **20**, 16566–16573.

© 2024 The Author(s). Published by the Royal Society of Chemistry

Open Access Article. Published on 10 December 2024. Downloaded on 2/10/2026 4:59:52 AM.
This article is licensed under a Creative Commons Attribution-NonCommercial 3.0 Unported Licence.

32 C.-T. Yang, J. Han, M. Gu, J. Liu, Y. Li, Z. Huang, H.-Z. Yu, S. Hu and X. Wang, *Chem. Commun.*, 2015, **51**, 11769–11772.
33 M. Starck, F. A. Laporte, S. Oros, N. Sisommay, V. Gathu, P. L. Solari, G. Creff, J. Roques, C. Den Auwer, C. Lebrun and P. Delangle, *Chem.–Eur. J.*, 2017, **23**, 5281–5290.
34 C. L. Fanny, A. Laporte, C. Vidaud and P. Delangle, *Chem.–Eur. J.*, 2019, **25**, 8570–8578.
35 L. L. Clainche and C. Vita, *Environ. Chem. Lett.*, 2006, **4**, 45–49.
36 L. Abou-Zeid, A. Pell, M. Garcia Cortes, H. Isnard, P. Delangle and C. Bresson, *Anal. Chim. Acta*, 2023, **1242**, 340773.
37 R. Pardoux, S. Sauge-Merle, N. Bremond, M. R. Beccia, D. Lemaire, C. Battesti, P. Delangle, P. L. Solari, P. Guilbaud and C. Berthomieu, *Inorg. Chem.*, 2022, **61**, 20480–20492.
38 D. A. Wappett and L. Goerigk, *J. Chem. Theory Comput.*, 2023, **19**, 8365–8383.
39 S. Grimme, J. Antony, S. Ehrlich and H. Krieg, *J. Chem. Phys.*, 2010, **132**, 154104.
40 A. V. Marenich, C. J. Cramer and D. G. Truhlar, *J. Phys. Chem. B*, 2009, **113**, 6378–6396.
41 P. W. Durbin, *Health Phys.*, 2008, **95**, 465–492.
42 M. Starck, N. Sisommay, F. A. Laporte, S. Oros, C. Lebrun and P. Delangle, *Inorg. Chem.*, 2015, **54**, 11557–11562.
43 F. Laporte, Y. Chenavier, A. Botz, C. Gateau, C. Lebrun, S. Hostachy, C. Vidaud and P. Delangle, *Angew. Chem., Int. Ed.*, 2022, **61**, e202203198.
44 A. Bavelloni, M. Piazzi, M. Raffini, I. Faenza and W. L. Blalock, *IUBMB Life*, 2015, **67**, 239–254.

© 2024 The Author(s). Published by the Royal Society of Chemistry